White Paper #9 – Satellite Views of the Tropical Pacific

Lindstrom, E.[1], Bourassa, M.[2], Chelton, D.[3], Corlett, G.[4] , Durland, T.[3], Farrar, T.[5], Janssen, P.[6], Lagerloef, G.[7], Lee, T.[8], Minnett, P.[8], O'Neill, L.[3], and Willis, J.[8]

[1] NASA Headquarters, United States
[2] Florida State University, United States
[3] Oregon State University, United States
[4] University of Leicester, United Kingdom
[5] Woods Hole Oceanographic Institute, United States
[6] European Center for Medium-Range Forecasts, United Kingdom
[7] Earth and Space Research, United States
[8] Jet Propulsion Laboratory, United States

1. Introduction

Satellites are an integral component of the Tropical Pacific Observing System (TPOS). Oceanographic satellite missions have been providing measurements for a suite of oceanographic variables such as sea surface temperature (SST), salinity (SSS), and height (SSH), as well as significant wave height (SWH), ocean surface wind speed and wind stress, precipitation, ocean mass, and variables related to ocean color (e.g., Chl). Combinations of satellite measurements also provide estimates of ocean surface currents and surface heat fluxes. These satellite observations have provided measurements of the tropical Pacific that are complementary to in-situ observations. For example, satellite altimetry and gravimetry in combination with Argo have enabled a comprehensive study of sea level and the relative contribution of steric and mass contributions. Satellites and mooring data together have greatly facilitated the estimation of upper ocean heat balance.

Satellites provide a unique vantage point to observe the tropical Pacific in many aspects. They have overall more uniform spatio-temporal sampling than *in situ* systems to capture oceanographic features. As such, they can help decipher eddy and large-scale signals from in-situ data such as measurements by Argo floats. The extensive spatial sampling also allows the calculation of spatial derivative fields important for the study of ocean and atmospheric circulation and air-sea interaction such as SST gradients and the surface wind stress curl and divergence. The more extensive (often global) coverage of satellites facilitates studies of large-scale teleconnections and impacts. On the other hand, in-situ data extend the interpretation of satellite data by providing information about vertical structure below the sea surface. They also help improve satellite observations by providing independent measurements critical to the calibration and validation of many satellite measurements. High-frequency measurements of some in-situ data (e.g., mooring and meteorological measurements) also help de-alias signals that may not be adequately sampled by satellites (e.g., diurnal signals).

This whitepaper summarizes the major contributions of satellites in studying the circulation and climate variability of the tropical Pacific (section 2), the advantages of the satellites and their complementarity to *in situ* observations (section 3), the unique capabilities of satellite observations of the ocean (section 3), and the need for the enhancement of future satellite observing systems to complement the design of the future tropical Pacific observing system (section 4).

2. Major contributions of satellites in observing the tropical Pacific

A diverse array of Earth-observing satellites has provided measurements of the globe, including the tropical Pacific for several decades. The current missions, along with missions already completed (e.g., TOPEX/Poseidon, JASON-1, NSCAT), have provided comprehensive measurements of several variables, including sustained measurements of SST for more than three decades, SSH for more than two decades, ocean surface wind speed for nearly three decades, and ocean surface vector winds for two decades. The upcoming missions continue and enhance the legacy of oceanographic satellite missions by extending the temporal record and by providing measurements with better sampling and/or accuracy (e.g., SWOT, RapidSCAT, and Sea and Land Surface Temperature Radiometer (SLSTR)).

The past and ongoing oceanographic satellite missions have made significant accomplishments. The major achievements related to ocean and climate research are summarized below and organized by different time scales. Although not discussed here, these satellite measurements have made important contributions to the improvement of models and climate prediction and to the study and forecast of shorter time-scale phenomena (covered by other whitepapers). The discussion here focuses on satellite measurements related to the physical state of the ocean, including meteorological forcing. Ocean color measurements are described in another whitepaper led by Dr Francisco Chavez.

Recommendation: Ensure all components, including satellites, *in situ*, models, data and information management are considered part of the observing system.

2.1 Intraseasonal variability

A spectrum of intraseasonal variability revealed by satellites

There are many different dynamical phenomena that occur at intraseasonal periods (20-100 days) in the tropical Pacific Ocean and the overlying atmosphere. In the ocean, the most prominent of these are tropical instability waves (TIWs) and equatorial Kelvin waves. Prominent modes of atmospheric intraseasonal variability include convectively coupled Kelvin waves and the Madden-Julian Oscillation (MJO). Intraseasonal variability in both the atmosphere and ocean stand out as prominent features in most data records in the tropical Pacific, and these various forms of intraseasonal variability have thus been the subject of intensive study with in situ and satellite measurements. We focus here on the uses and limitations of satellite measurements for studying and monitoring intraseasonal variability in the ocean; representative examples of the use of satellite observations for study of atmospheric intraseasonal variability include Madden and Julian (1994), Wheeler and Kiladis (1999), and Roundy and Frank (2004).

Several distinct types of oceanic variability co-exist with intraseasonal periods, including eastward propagating Kelvin waves, and shorter-wavelength, westward-propagating variability such as TIWs. A relatively clear separation of these processes is often achieved through examining the spectrum of oceanic variability in the zonal-wavenumber-frequency domain. Examination of the zonal-wavenumber/frequency spectrum is also helpful because the most common theoretical approaches to Kelvin waves and TIWs are carried out in the zonal-wavenumber/frequency domain. As is discussed further below, spectra of different oceanic properties tend to highlight different wavenumber-frequency bands; we will examine the zonal-

wavenumber/frequency spectrum of SSH (Perigaud, 1990; Zang et al., 2002; Wakata, 2007; Farrar, 2008; Shinoda et al., 2009; Farrar, 2011). The zonal-wavenumber/frequency spectrum of SSH exhibits two broad regions of elevated SSH variance, one corresponding to eastward propagating Kelvin waves at small, positive zonal wavenumbers (wavelengths exceeding 50° longitude), and one corresponding to TIWs and other westward-propagating variability with zonal wavelengths of about 9-30° (Figure 2.1). The SSH spectrum shown in Figure 2.1 (after Farrar, 2011) was estimated using data from the AVISO gridded altimetry product over the period 1993-2006 and almost the full width of the equatorial Pacific (149°E-88°W).

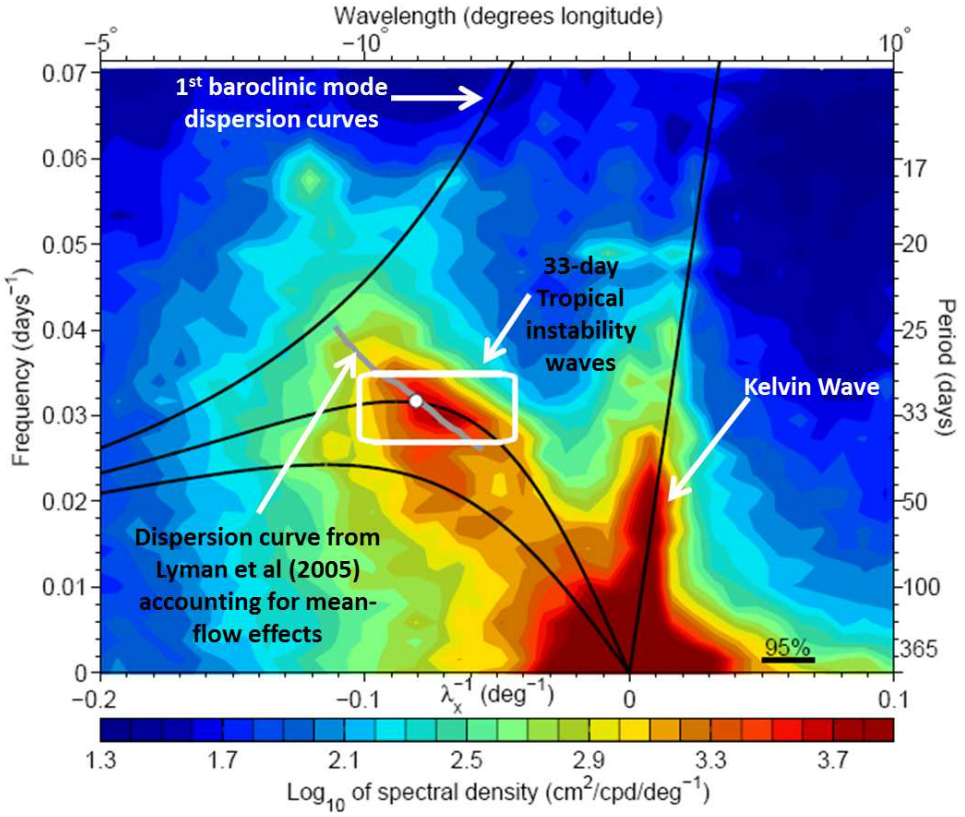

Figure 2.1 - Zonal-wavenumber/frequency spectrum of SSH, averaged over 7°S-7°N (after Farrar, 2011), using data from 1993-2006 and almost the full width of the Pacific (149°E-88°W). At periods of 20-100 days, there are two broad regions of elevated SSH variance, one corresponding to eastward propagating Kelvin waves at small, positive wavenumbers (wavelengths exceeding 50°), and one corresponding to TIWs and other westward-propagating variability having zonal wavelengths of about 9-30°. The TIW spectral peak in SSH near 33-day periods (white box) has wavelengths of 12-17°. The four black curves are the theoretical dispersion curves for the first-baroclinic-mode Kelvin, Rossby, and mixed Rossby-gravity waves. The grey line depicts a theoretical dispersion curve for the unstable TIW mode, and the white circle indicates the fastest growing wavelength (from Lyman et al., 2005). The 95% confidence interval should be measured against the color scale; a difference of two contour intervals is significant at 95% confidence.

TIWs provide a natural starting point for a discussion of the use of satellite measurements for the study of intraseasonal variability because they were first discovered in satellite infrared SST measurements in the Pacific (Legeckis, 1977). TIWs arise from instabilities of the equatorial

current system (Philander, 1976; Luther and Johnson, 1990; Lyman et al., 2005), and are clearly visible in satellite SST measurements as a meandering of the northern side of the equatorial cold tongue near 2°N. More recently, microwave SST measurements were used to show that TIWs also cause SST signals on the southern side of the equatorial cold tongue, near 2°S (Chelton et al., 2000; Figure 2.2).

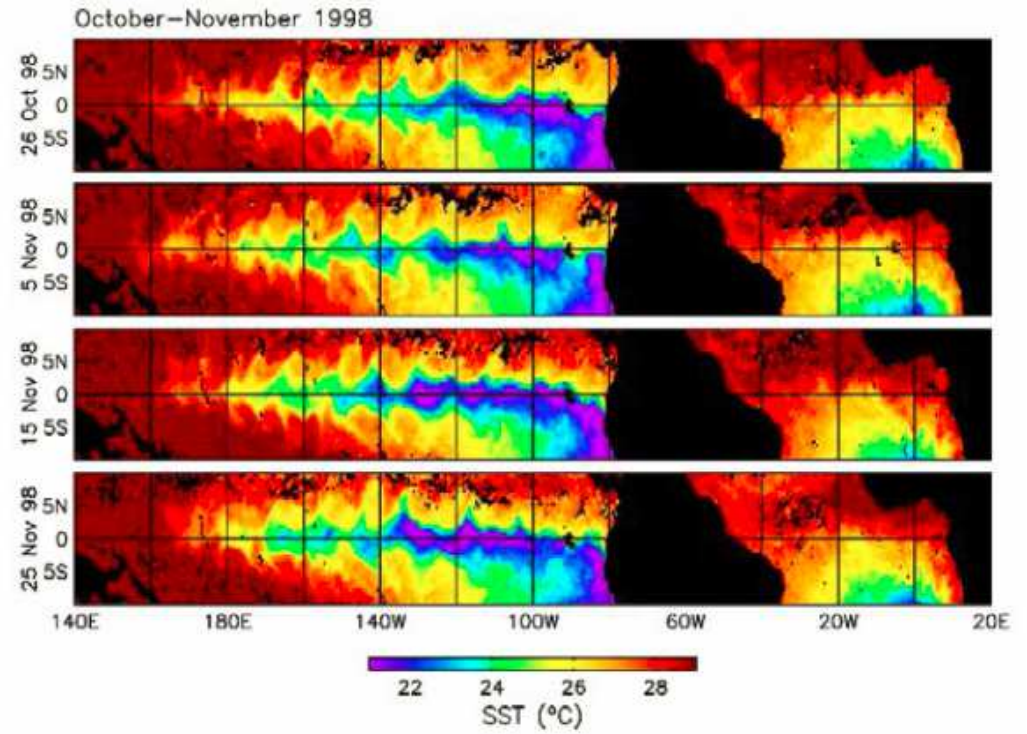

Figure 2.2 - SST measurements from the Microwave Imager onboard the Tropical Rainfall Measuring Mission (TRMM) satellite. Tropical instability waves produce the cusp-shaped patterns along the northern and southern SST fronts of the tongue of cold water on the equator (Chelton et al., 2000).

The discovery of TIWs in the late 1970's stimulated a great deal of subsequent theoretical and observational work to understand their generation mechanisms, properties, and consequences. Descriptions of the properties of TIWs have varied widely: TIWs have been reported to occur at periods of 14-50 days, zonal wavelengths of 7-25°, and to have maximum amplitude at locations ranging from the equator to 6°N (Qiao and Weisberg, 1995). Observational studies of TIWs have typically characterized them as a fairly narrowband phenomenon, but this apparently conflicts with the broad range of wavenumbers and frequencies reported. For example, Halpern et al. (1988) characterized the TIW signal in meridional velocity measurements on the equator as a narrowband fluctuation with a period of 20 days, while Lyman et al. (2005) found a clear maximum in SSH variability at periods of about 33 days.

When the various wavenumbers and frequencies that have been reported or theoretically predicted for TIWs are plotted over the spectrum shown in Figure 2.1, it becomes apparent that the various estimates collectively span the range of wavenumber-frequency space that exhibits energetic SSH variability in the 7°S-7°N latitude band (Figure 2.3). Figure 2.3 includes the wavenumber-frequency estimates summarized in Table 1 of Qiao and Weisberg (1995) and some more recent estimates from Chelton et al., (2000), Donohue and Wimbush (1998),

McPhaden (1996), and Lyman et al., (2005, 2007). The figure shows boxes, lines, and points depending on whether each study provided a range of wavenumbers and/or frequencies or simply stated a single wavenumber and frequency. Not surprisingly, previous studies using SSH measurements (Perigaud, 1990; Lyman et al., 2005) identified TIW wavenumbers and frequencies around the spectral peak in SSH seen near 33-day periods. Those studies, and other SSH-based studies by Farrar (2008, 2011) and Shinoda et al. (2009) also determined the peak TIW variability to occur near 5°N. At the other extreme of the reported frequency range, in situ equatorial velocity measurements have tended to yield shorter reported periods, near 20 days, and they have tended to see the strongest signals in meridional velocity on the equator (e.g., Halpern et al., 1988). Satellite SST and in situ temperature measurements have tended to yield estimates in between these two extremes and have also tended to identify maximum variability as occurring near 2°N. One interpretation of these disparate observations is that there is TIW variability that resembles mixed Rossby-gravity waves, which have a relatively weak SSH signal and a strong signal in equatorial meridional velocity, and other variability that resembles first-meridional-mode (and perhaps second-meridional-mode) equatorial Rossby waves, with a stronger off-equatorial SSH signal (Lyman et al., 2007).

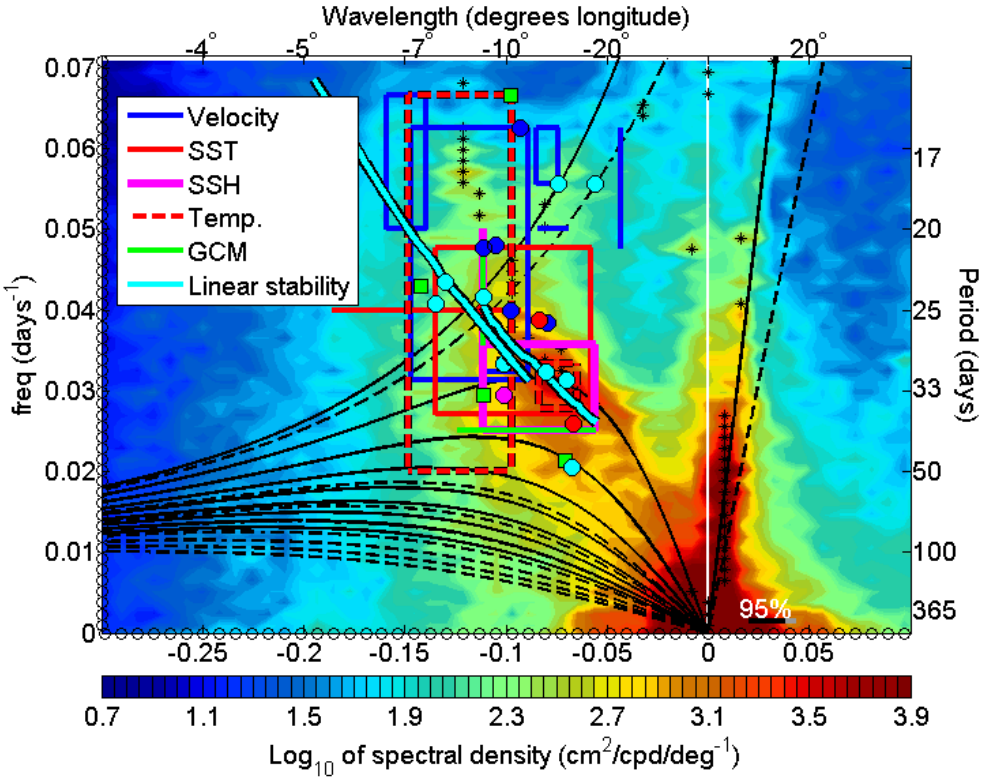

Figure 2.3 - A zonal-wavenumber/frequency spectrum of SSH similar to the one in Figure 2.1, but averaged over 5°S-5°N. Previous estimates of the wavenumbers and frequencies of tropical instability waves (TIWs) are indicated, where a box indicates that a particular study provided a range of wavenumbers and frequencies, a line indicates a range of frequencies or wavenumbers, and a point indicates that a single wavenumber-frequency value was given. “SST” and “SSH” are from satellite observations, and “Velocity” and “Temp” are from moored in situ measurements.

Previous studies of TIWs using satellite observations were mostly based on SST, SSH, wind, and ocean color. SSS observations from the Aquarius/SAC-D satellite mission have provided an unprecedented opportunity to study the salinity structure associated with TIWs. The studies by Lee et al. (2012) demonstrated the capability of Aquarius data in detecting tropical Pacific TIWs and the complementarity between SSS and other satellite observations in studying the TIWs. In particular, SSS provide the strongest propagating signature of tropical Pacific TIWs near the equator where the salty South Pacific waters meet the freshwater waters under the ITCZ, forming a relatively large meridional SSS gradient. In contrast, the meridional gradient of SST is weaker near the equator and is the strongest near the northern edge of the cold tongue near 2N, where TIW signature in SST is strongest. For SSH, the strongest signature is further north near the center latitudes of the tropical instability vortices. Aquarius data are not only able to detect TIWs, but reveal new features of the TIWs not previously reported from SST and SSH observations. The dominant westward propagating speed of TIWs near the equator is approximately 1 m/s, which nearly twice as fast as the approximately 0.5 m/s dominant speed reported from SST and SSH data, typically off the equator. This is because the dominant periods of TIWs near and away from the equator are 17 and 33 days, and are associated with the projection of instabilities onto the Yanai mode and the Rossby mode, respectively (Lyman et al., 2007). Satellite SSS allows a better characterization of TIWs near the equator because of the relatively large meridional SSS gradient near the equator (in contrast to the strong SST gradient away from the equator near the cold-tongue edges). The new discovery has important implications to eddy-mean flow interaction and eddy-induced mixing.

Kelvin waves are the other major form of intraseasonal variability in the tropical Pacific Ocean. These waves are visible in Figures 2.1 and 2.3 as a low-wavenumber band of high variance along the first-baroclinic-mode Kelvin wave dispersion curve. They dominate the variance of SSH and other fields at 30-90-day periods and have received considerable attention (e.g., Enfield, 1987; McPhaden and Taft, 1988; Johnson, 1993; Johnson and McPhaden, 1993; Kessler et al., 1995; Kessler and McPhaden, 1995; Hendon et al., 1998; Kutsuwada and McPhaden, 2002; Zang et al., 2002; Cravatte et al., 2003; Roundy and Kiladis, 2006; Farrar, 2008). The waves are forced by intraseasonal wind fluctuations (e.g., from the MJO) in the western and central Pacific (Kessler et al., 1995; Hendon et al., 1998).

Air-sea coupling associated with tropical instability waves

Satellite observations of SST and surface vector winds have provided a clearer understanding of air-sea interaction in the eastern tropical Pacific than could be obtained from TAO mooring data or model wind fields. SST anomalies on scales shorter than ~1000 km modify the turbulent mixing and pressure field within the marine atmospheric boundary layer. This results in local changes in surface winds and stress from imbalances between the turbulent stress divergence and pressure gradient forces that generate accelerations of surface winds from cool to warm water and decelerations from warm to cool water. This coupling between SST and surface stress is easily identified in association with tropical instability waves (TIWs) (e.g., Liu et al., 2000; Chelton et al., 2001; Polito et al., 2001; Hashizume et al., 2002; Chelton, 2005). The divergence of the surface stress is found to be a linear function of the downwind component of the SST gradient; the curl of the surface stress is likewise found to be a linear function of the crosswind component of the SST gradient (Chelton et al., 2001). Wind stress divergence and

curl anomalies propagate westward in lock step with the downwind and crosswind SST anomalies associated with the westward propagating TIWs (Chelton et al., 2001; Chelton, 2005). This SST influence on surface wind stress fields is evident in model winds such as the operational ECMWF analyses of 10-m winds, but with coarser resolution and with air-sea coupling that is too weak by about a factor of two (Chelton, 2005).

Because the wind stress curl is correlated with the crosswind SST gradient, the feedback effects of Ekman upwelling are strong where the winds blow parallel to isotherms. This SST-induced Ekman upwelling consists of order-1 perturbations of the large-scale background Ekman upwelling. Since their persistence time scales are weeks or longer, the small-scale features in the wind stress curl field are important to the ocean circulation. For example, a zonal band of strong wind stress curl just north of the equatorial cold tongue that is established in the time-averaged wind stress curl field from the influence of SST on surface wind stress (Chelton et al., 2001) significantly increases the transport of the northern branch of the South Equatorial Current (Kessler et al., 2003).

The ramifications of this 2-way coupling have been investigated by Pezzi et al. (2004) from an ocean model of TIWs in the Pacific Ocean with empirical coupling consistent with the satellite observations. The coupling resulted in a modest (~10%) but significant negative feedback on TIWs that reduced the temperature and meridional velocity variability and dampened the growth rate of the TIWs. The net effects of these changes were to decrease the meridional fluxes of heat and momentum, thereby altering the mean state in a manner that resulted in moderate cooling of the equatorial cold tongue and strengthening of the Equatorial Undercurrent. Similar results have been obtained from a full-physics coupled model that was run for 7 years to investigate TIWs in the Atlantic (Seo et al., 2007b).

Another empirically coupled model of the tropical Pacific Ocean concludes that the feedback effects of TIW-induced SST variations of the wind stress field may also be important to El Niño-Southern Oscillation (ENSO) variability (Zhang and Busalacchi, 2008; 2009). The cooling of the equatorial cold tongue by the 2-way coupling can modulate the amplitude and timing of transitions between the El Niño and La Niña phases of the ENSO cycle. The TIW-induced coupling between SST and wind stress may therefore contribute to the observed irregularity of ENSO variability.

2.2 Seasonal variability

Satellite observations have also enhanced the knowledge about the variability of the tropical Pacific Ocean on seasonal time scales. One particular example is the quasi-annual equatorial Rossby wave in the tropical Pacific Ocean. The classical theory for equatorially trapped waves, in which the equations of motion for a given vertical mode are linearized about a state of rest on an equatorial beta plane, yields an orthogonal basis set of meridional modes with latitudinal structures of the pressure and the two components of velocity that can be expressed in terms of linear combinations of Hermite functions (e.g., Moore and Philander, 1977). At low frequencies, the first vertical mode, first meridional mode that is often presumed to account for most of the westward propagating variability has a phase speed of ~0.9 m/s. The pressure perturbations associated with this theoretical mode are symmetric about the equator. This latitudinal structure is not observed in the Pacific Ocean. Studies of annual variability in subsurface thermal data

and in altimeter data consistently find asymmetric latitudinal structure with larger amplitude north of the equator. These studies also consistently find a westward propagation speed about half as fast as predicted by the classical theory.

The observed latitudinal asymmetry (Figure 2.4) has been variously attributed to sampling errors in the observational data, a superposition of multiple meridional Rossby wave modes, asymmetric forcing by the wind, and forcing by cross-equatorial southerly winds in the eastern Pacific. Chelton et al. (2003) showed that, when the equations of motion are linearized about mean zonal currents typical of the equatorial Pacific, the latitudinal pressure structure for the first meridional mode is distorted in a manner that agrees well with altimeter measurements of SSH variability (Chelton et al, 2003; Durland et al., 2011). The classical double-peaked symmetric structure becomes one in which the northern peak is roughly twice as large as the southern one as a consequence of the modification of the potential vorticity gradient by meridional shear in the equatorial current system. The mean currents for this study were derived from ADCP data obtained during cruises to service the TAO-TRITON moorings.

The background mean currents also decrease the westward phase speed of the first meridional mode, improving the consistency with the observations. This is partly through eastward advection by the Equatorial Undercurrent, and partly through a decrease in the background potential vorticity gradient at the peaks of the South Equatorial Current, which coincide with the latitudes where the first-mode meridional velocity has extrema (Durland et al., 2011).

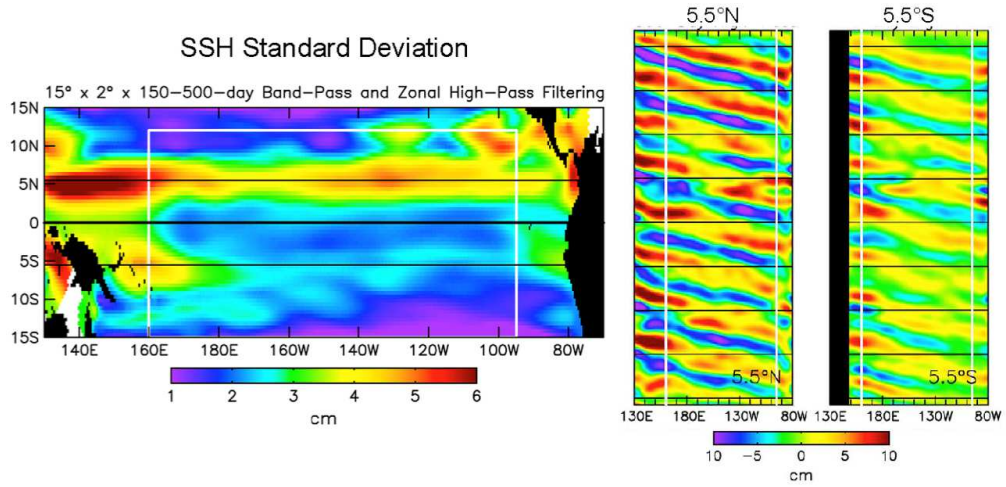

Figure 2.4 - Standard deviation of seasonal SSH in the tropical Pacific (left) and the propagation of the seasonal SSH at 5.5°N and 5.5°S (right), showing strong latitudinal asymmetry of the quasi-annual Rossby waves and phase speed that are much slower than that predicted by linear theory, suggesting the roles of wind forcing and ocean currents.

The fact that equatorial winds do not exhibit a westward phase propagation at the latitude of the largest SSH peak initially led to some confusion as to the whether the wave is directly forced throughout the basin. Durland and Farrar (2012) showed that the efficiency of the wind forcing depends on how the meridional structure of the zonal wind projects onto the meridional structure of the zonal velocity field associated with the free wave. In contrast to the SSH eigenfunction that has extrema at about 5°N and 5°S, the eigenfunction of zonal velocity for the first meridional mode has an extremum on the equator in the classical theory. When the effects

of mean currents are taken into account, the zonal velocity extremum becomes displaced only slightly north of the equator. Although the annual zonal winds on the equator are considerably weaker than those in the ITCZ and SPCZ, the annual harmonic of zonal wind stress in the equatorial Pacific calculated from the satellite scatterometer-based climatology of Risien and Chelton (2008) exhibits a westward phase propagation within a few degrees of the equator, where it can project well onto the oceanic mode that crosses the basin in roughly one year. The phase speed of the zonal wind varies with latitude and longitude, but on the equator between 100°W and 170°E, it averages about 0.47 m/s, in rough agreement with the phase speeds estimated from altimeter data by Chelton et al. (2003) for the annual SSH variability. The evidence based on altimeter and scatterometer data thus strongly suggests an oceanic wave that is resonantly forced by the zonal winds across the entire equatorial Pacific. This agrees with conclusions of pre-satellite studies of the vertically propagating annual Rossby wave (Lukas and Firing, 1985; Kessler and McCreary, 1993), although these studies were unable to account successfully for the latitudinal asymmetry in the variability.

Questions remain regarding details of latitudinal and longitudinal variability in the measured SSH phase speed. Variations in the zonal wind propagation speed are likely to be important. It is also possible that a superposition of meridional modes plays a role. Durland et al. (2011) showed that the mean currents of the equatorial Pacific also produce an asymmetry in the eigenfunctions of the second meridional mode, and that the westward phase speed of this mode is increased by the mean currents. This is in contrast to the 1st meridional mode, for which the phase speed is decreased by the mean currents, as noted above. The phase speeds of the two gravest meridional modes are thus brought closer together in the mean-current-modified system, and the likelihood is increased that the annual winds could resonantly excite both modes simultaneously. Such a mode superposition would alter the observed phase speed at particular latitude, and lead to discrepancies between observed phase speeds at different latitudes, which are at least qualitatively consistent with the analysis of altimeter data by Chelton et al. (2003).

2.3 Interannual variability

In addition to the contribution to the understanding of the seasonal cycle to which ENSO events are phase-locked, satellite observations of SST, SSH, surface currents, and wind have become indispensable resources to monitor, understand, and even predict interannual variability of the tropical Pacific. For example, satellite observations have provided a multi-variable, basin-scale view of the evolution of El Niño, La Niña, and their transitions, and the associated ocean-atmosphere interaction (e.g., Picaut et al., 1996, McPhaden et al., 1998). Satellite-derived ocean surface currents (OSCAR, http://oscar.noaa.gov) were used to show that the first EOF of the surface currents leads that of SST by 2-3 months in the tropical Pacific (Figure 2.5), suggesting the important role of ocean currents in regulating ENSO-related SST (Lagerloef et al., 2003; Lumpkin et al., 2013).

Satellite observations have also improved the understanding of ENSO diversity in the past three decades, such as the different behaviors of the so-called central- and eastern-Pacific El Niño and their low-frequency change (e.g., Lee and McPhaden 2010). The strongest central-Pacific El Niño thus far occurred in 2009-10 (Lee and McPhaden 2010). It had a substantial impact on

the South Pacific and West Antarctica (Lee et al., 2010, Boening et al., 2011).

Satellite-derived SSH and wind stress data have been used to characterize the structure and variability of the lower branch of the so-called subtropical cell (STC), i.e., a shallow overturning cell that connects the tropical and subtropical oceans (e.g., Lee and Fukumori, 2003). SSH differences between the eastern and western boundary are used as a proxy for the net meridional geotrophic transport in the pycnocline, which is the lower branch of the STC. The structure of SSH and wind stress curl in the western tropical Pacific suggest near anti-correlated variability of pycnocline geostrophic flow near the western boundaries and in the interior, with the former being more dominant. This feature is due to the anomalous horizontal circulation generated by wind stress curl in the western tropical Pacific, as shown from satellite-based estimates of wind stress curl associated with the variability of the Intertropical Convergence Zone (ITCZ) and the South Pacific Convergence Zone (SPCZ). The boundary and interior flow of the Pacific STC therefore play opposite roles in regulating the interannual variability of upper ocean heat content in the tropical Pacific Ocean.

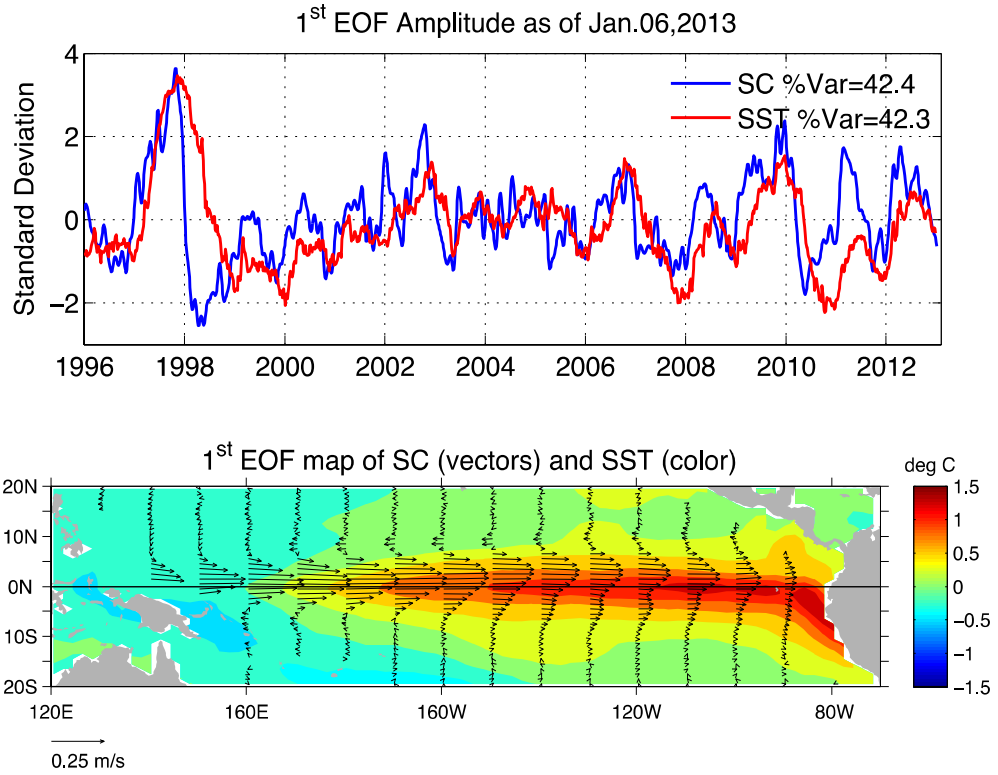

Figure 2.5 - The time series (upper) and spatial structure (lower) of the first EOF of non-seasonal ocean surface current and SST in the tropical Pacific, showing the 2-3 month lead time of the surface current over SST (after Lumpkin et al., 2013).

Satellite observations of SST are essential in the study of interannual variability of the mixed-layer heat balance because they enable the calculation of horizontal gradient of SST needed in the calculation of the horizontal heat advection in addition to the related estimate of SST tendency (e.g., Wang and McPhaden, 2000; Zhang and McPhaden, 2010).

2.4 Decadal and longer variability

Despite the relatively short temporal records, satellite observations have provided important observations and insights about decadal variability in the tropical Pacific. Satellite observations of SSH and wind stress reveal a near coherent decadal change over much of the Indo-Pacific region (including the subpolar North Pacific and the Southern Ocean) since the early 1990s that is substantially stronger than that observed previously (Lee and McPhaden 2008). Satellite observations of zonal wind stress and the SSH difference between the eastern and western boundaries allow an estimate of the decadal variability of the strengths of the upper and lower branches of the STC, respectively. Based on these, Lee and McPhaden (2008) suggest that the STCs of the Pacific and Indian Ocean are linked by an atmospheric bridge (through the oscillation of the Walker Circulation) and an ocean tunnel (via the connection of the Indonesian Archipelago). The Pacific and Indian Ocean STCs oscillate out of sync during this period, thus playing opposite roles in controlling the upper ocean heat content of the Indo-Pacific domain. This has strong implications to ocean-atmosphere coupling of the Indo-Pacific region on decadal time scales (at least during the period of the satellite observations).

Satellite observations of SST in the past three decades reveal a statistically significant increasing trend of the amplitude of El Niño in the central Pacific, which the amplitude nearly doubled in the past three decades (Lee and McPhaden, 2010). This is associated with the more frequent occurrence of a stronger central-Pacific El Niño. The trend of El Niño amplitude in the central equatorial Pacific is in stark contrast to the amplitude of eastern-Pacific El Niño that shows no significant trend. Lee and McPhaden (2010) also showed that, while the El Niño amplitude in the central-Pacific has been increasing over the past three decades, no significant trend is found in La Niña amplitude and SST during neutral years in this region. Therefore, the increasing amplitude of El Niño in this region contributed to the well-observed increasing trend of the background SST.

3. Unique vantage point from space and complementarity with in-situ observations

Satellite systems have important advantages in observing the tropical Pacific in several aspects. For instance, the overall more uniform spatio-temporal sampling of satellite observations in comparison with in-situ data helps decipher large-scale and eddy variability captured by in-situ data such as Argo floats (e.g., Willis et al., 2003; Willis 2010).

The relatively more uniform and dense spatial sampling of many satellite observations compared with in situ observations allows the calculation of spatial derivative fields. Satellite SST, SSS, and wind-stress gradients can be computed with much finer spatial resolutions than those obtained from in-situ data, facilitating the analysis of mixed-layer heat and salt budgets and ocean dynamics. The importance of derivative SST and wind stress fields for studies of air-sea interaction was discussed in Sec. 2.1. In the case of SSS, the Aquarius satellite launched in 2011 has revealed much finer salinity gradients than those estimated from the Argo data (Figure 3.1).

The extensive (often global) spatial coverage of satellite observations is critical to studies of basin-to-global-scale teleconnections and the related impacts. For example, Lee et al. (2010) illustrated the teleconnection between the tropical Pacific (especially during the 2009-10 central-

Pacific El Niño) and the Southern Ocean and Antarctica (including the SST near the Wilkins Ice Shelf). Boening et al. (2012) documented the large effect of the 2011 La Niña on globally averaged sea level and the relation to the record-flooding event in Australia.

Complementarity between satellite and in-situ observations has been shown by a large number of studies. In particular, in-situ data have played important roles in many applications of satellite data, primarily by providing information about subsurface variability that cannot be obtained from satellites. For example, satellite data from altimeters and GRACE have been used in combination with in-situ Argo data to study the nature of sea level changes, in particular, the steric and mass contributions (e.g., Willis et al. 2003; Willis et al. 2008). SST derived from satellites, and the TOGA-TAO arrays have been used to produce the widely used blended OISST (e.g., Reynolds et al., 2007). Other examples of this complementarily were discussed in section 2.

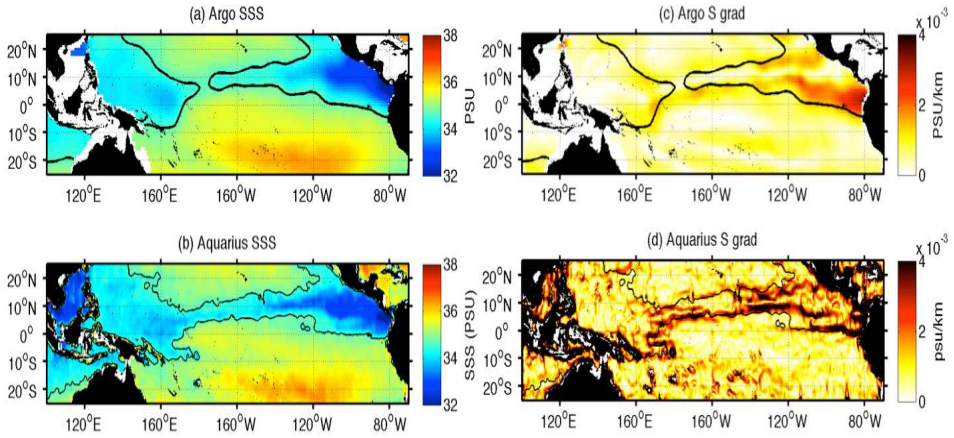

Figure 3.1 - Aquarius SSS gradients reveal intense frontal structures that are not evident in Argo OI maps. The dark contour is the 34.6 isohaline (Courtesy of Lagerloef, G., and Kao, H.).

Despite their relatively uniform spatio-temporal coverage, satellite observations have a number of limitations. For example, satellite observations are prone to high-frequency aliasing between temporal samples, in contrast to mooring observations that have high frequency sampling. Satellite infrared observations are prone to large sampling errors in the tropics from missing data because of the persistent cloud cover in many regions that obscures the sea surface at infrared wavelengths. As summarized below, infrared estimates of SST are also subject to measurement errors from several sources of atmospheric contamination of the measurements. Satellite microwave measurements are much less affected by atmospheric contamination. Moreover, because clouds are transparent at microwave frequencies, sampling errors are also less for microwave data than for infrared data. Sampling errors can nonetheless be an issue in microwave data because of affects of rain contamination. As discussed below, temporally and spatially averaged microwave data are therefore biased toward non-raining conditions.

In-situ data, including measurements from the TAO-TRITON array, have historically been an important component for the global calibration and validation of a suite of satellite data (e.g., SST, SSS, wind, precipitation). High-frequency mooring observations may be used to de-alias high-frequency signals not adequately captured by satellites (e.g., diurnal variability), at least regionally near the moorings. The following discussion illustrates some examples of the use of

in-situ data for the calibration and validation of satellite data.

3.1 SST validation

Satellite measurements of SST by infrared sensors, especially in the tropics, have a significant sampling issue because cloud cover obscures the sea surface at infrared wavelengths. In cases of low-level clouds, especially at nighttime, a large source of error in infrared estimates of SST is errors in the cloud masking algorithms. In such cases, clouds are difficult to detect because they often have a temperature very similar to that of the sea surface. Infrared SST retrievals are also subject to large errors from water vapor, which is a bigger problem in the tropics than anywhere else in the world ocean. Infrared estimates of SST are also contaminated by aerosols (which occur for a variety of reasons, including volcanic eruptions, dust storms and smoke from agricultural and forest burning). Aerosol concentrations are often large in the tropics. Since the tropics are especially prone to all of these sources of errors, TAO data have been very useful for improving infrared SST retrieval algorithms.

Satellite microwave measurements are much less affected by atmospheric effects. Whereas atmospheric transmittance is typically less than 50% and sometimes less than 10% at the wavelengths used for infrared estimates of SST, it is more than 97% at microwave frequencies, even in conditions of very high water vapor. As noted above, however, microwave measurements cannot be made in raining conditions. In most cases, it is easy to identify and therefore flag rain contaminated microwave data. The biggest problem is thus that the data gaps result in sampling errors, as opposed to the combined measurement and sampling errors in the infrared data. Although the data gaps in microwave data are much less of a concern than data gaps from cloud cover in the infrared measurements, they are nonetheless significant.

The most stringent accuracy and stability requirements on satellite-derived SSTs are imposed by climate research and monitoring purposes (Interim SST Science Team White Paper, 2010; Kaiser-Weiss et al., 2012). Over scales of order 100km, the absolute accuracy requirement is ± 0.1K and the stability requirement is ±0.04 K decade^{-1} (Ohring et al. 2005; Kaiser-Weiss et al., 2012). Not only is it very challenging to achieve these accuracies using either in situ or satellite measurements, it is also very difficult to demonstrate whether these targets have been met. The generation of Climate Data Records (CDRs) requires contributions from several satellite instruments over time (NRC, 2000; NRC, 2004). The generation of temperature CDRs is greatly facilitated by the fact that temperature is one of the seven base units of the Système International d'Unités (SI) to which measurements should be referenced (BIPM, 1995); this provides the basis for combining measurements from several different sources.

Assessing uncertainties by simple comparisons between SST fields from different satellite instruments does not necessarily satisfy the accuracy and stability requirements, even for the case of multiple instruments on satellites that are contemporaneous or have temporally overlapping missions. One exception is the use of measurements from the ATSR and AATRS series ((Advanced) Along-Track Scanning Radiometer; see below) to bias correct contemporaneous AVHRR (Advanced Very High Resolution Radiometer) SSTs (O'Carroll et al., 2012). There are several approaches to validating the satellite retrievals of SST using independent measurements, with each source of validating data having their own strengths and weaknesses (Minnett, 2010). The most plentiful source of validating data is the drifting buoy

array that comprises about a thousand buoys reporting near surface temperature per day (Figure 3.2); the depths of the drifting buoy measurements are typically 0.2 - 0.3 m.

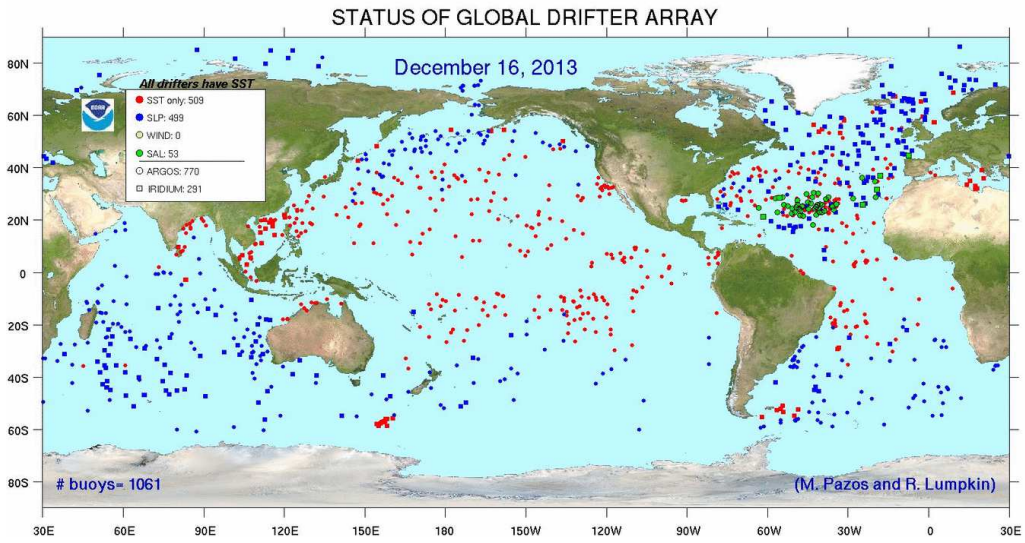

Figure 3.2 - Distribution of drifting buoys, all of which report near surface temperature.

The accuracy of SST from drifters is in the range 0.15 – 0.4 K (O'Carroll et al., 2008; Xu and Ignatov, 2010; Merchant et al., 2012) and therefore has uncertainties greater than the CDR requirements. There are efforts underway, through the Group for High Resolution SST (GHRSST) and the Data Buoy Cooperation Panel (DBCP), to improve the accuracy of the temperatures measured from drifters by about an order of magnitude.

The Global Tropical Moored Buoy Array (GTMBA) near-surface thermometers are calibrated before and after deployment and have a stated accuracy of 0.01K (Gentemann et al. 2004). Therefore, at least in principle, the GTMBA temperatures can make a useful contribution to the assessment of satellite-derived SST uncertainties in the tropical Pacific; modeling is required to remove the effects of diurnal heating and the thermal skin layer between the surface and the drifting buoy measurement depth (Embury and Merchant, 2012a; Embury et al., 2012b).

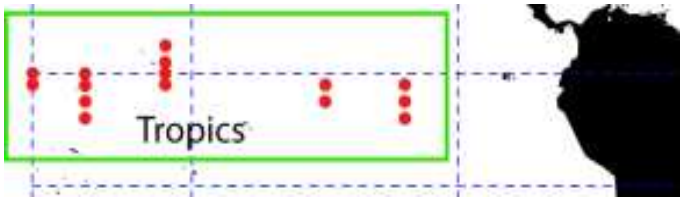

Figure 3.3 - Location of 'primary' GTMBA moorings identified by Merchant et al. (2012) as being suitable for assessing the stability of the ATSR and AATSR SST record.

The pre-deployment calibration of thermometers on the Argo profilers is rigorous and the instrument is designed to be very stable. Thus, the near-surface temperatures from Argo, especially from the "unpumped" sensors, have the potential to contribute to the assessment of satellite-derived SSTs (Castro et al., 2014).

Only one assessment of stability capable of being informative at the level required by Ohring et al. (2005) has been published (Merchant et al., 2012) which assesses the stability of the

(A)ATSR satellite SSTs relative to the GTMBA measurement. Only GTMBA buoys with a minimum of 120 months of data in the period 1991–2009 were used, and only buoys that passed strict quality control procedures were accepted. The resulting set of 'primary' GTMBA for stability assessment is shown in Figure 3.3.

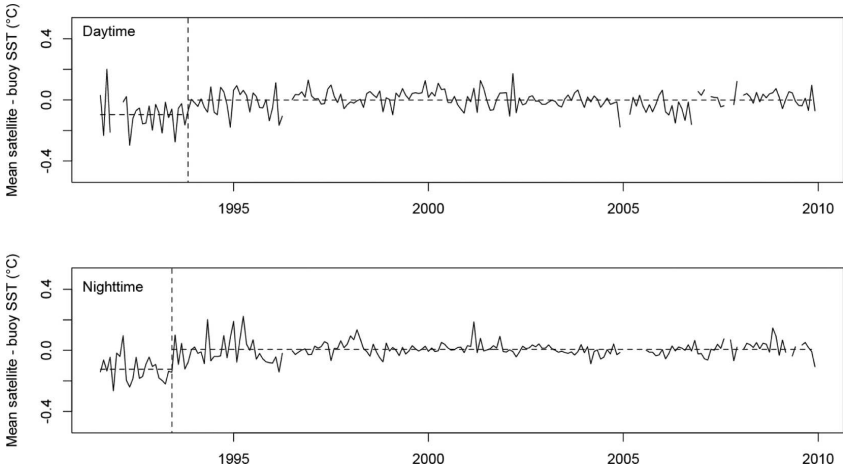

Figure 3.4 - Time series of monthly mean SST differences between ARC and GTMBA SSTs (taken from Merchant et al., 2012). See manuscript for further details and explanation of plot.

The monthly mean composite time series for daytime and nighttime (A) ATSR SST_{1m} data minus co-located GTMBA SSTs shown in Figure 3.4. The 95% confidence intervals for the trends are -0.0026 to 0.0015 K yr^{-1} (daytime) and -0.0018 to 0.0019 K yr^{-1} (nighttime). These results suggest that the (A) ATSR SSTs meet the target stability required by Ohring et al. (2005) in the tropics from 1994 onward. The use of the GTMBA for stability assessment is now an essential part of activities to analyze long-term satellite derived SST records. As such the GHRSST Climate Data Assessment Framework (CDAF) has this as a core activity. Such analyses are highly dependent on the long-term continuity of the GTMBA, particularly at the locations with the longest available data records such as the locations emphasized in Figure 3.4.

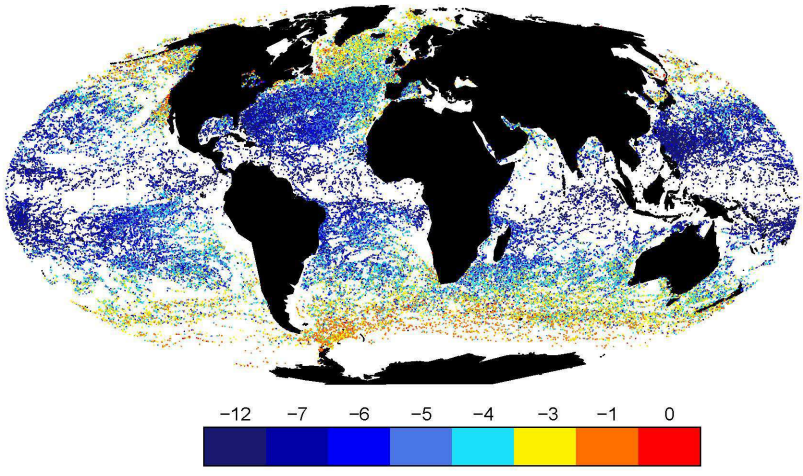

Figure 3.5 - VIIRS night-time temperature deficit at 11 µm, with reference to drifting and moored buoys. January 2012 to September 2013.

The paucity of measurements from drifting buoys in the tropics apparent in Figure 3.3 is a persistent feature. Figure 3.5 shows the global distribution of the difference between the 11µm brightness temperature measured by Visible Infrared Imaging Radiometer Suite (VIIRS) and in situ temperatures measured from drifting and moored buoys in confidently cloud-free conditions for most of the *Suomi* National Polar-orbiting Partnership (S-NPP) mission (January 2012-September 2013). It is clear that for much of the equatorial regions, the only in situ data are from the GTMBA – this is especially apparent in the Pacific Ocean.

The ITCZ poses particular challenges to the measurement of SST, because of the persistence of the clouds obscuring the surface to infrared radiometers, and rainfall contaminating the passive microwave measurements (Figure 3.6). There is a pronounced sampling minimum in the equatorial Pacific and Tropical Warm Pool regions, which underscores the need for continuing GTMBA measurements.

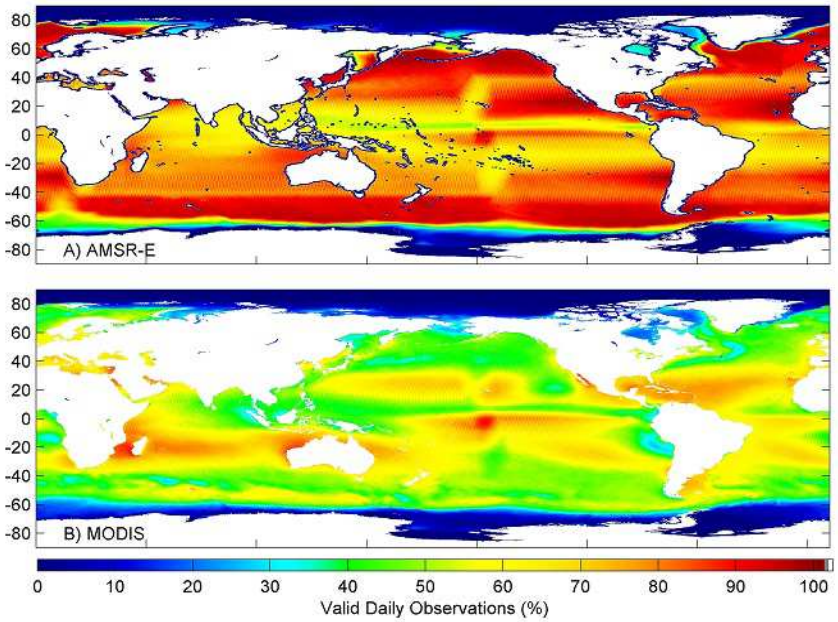

Figure 3.6 - Global distributions of the long-term fraction of SST retrievals in microwave measurements (AMSR-E top) and infrared measurements (Aqua MODIS, bottom) (figure provided by Gentemann, C.L., Remote Sensing Systems).

The effects of the cloud obscuration in infrared SST fields can be mitigated to some extent by temporal or spatial averaging, but the effects of sampling errors cannot be entirely eliminated in regions of persistent clouds. Figure 3.7 shows the consequences of clouds for daytime and night-time measurements. These are averages for January, April, July, and October 2011. The effects of spatial and temporal averaging are different, but a persistent feature is a negative bias in the equatorial regions in the eastern Pacific and eastern Atlantic Oceans. These are associated with equatorial upwelling and TIWs on the zonally aligned fronts to the north and south of the upwelling features. Clouds form preferentially on the warm sides of the fronts (Legeckis, 1977) leading to persistent and significant negative biases from sampling errors in the satellite-derived infrared SSTs.

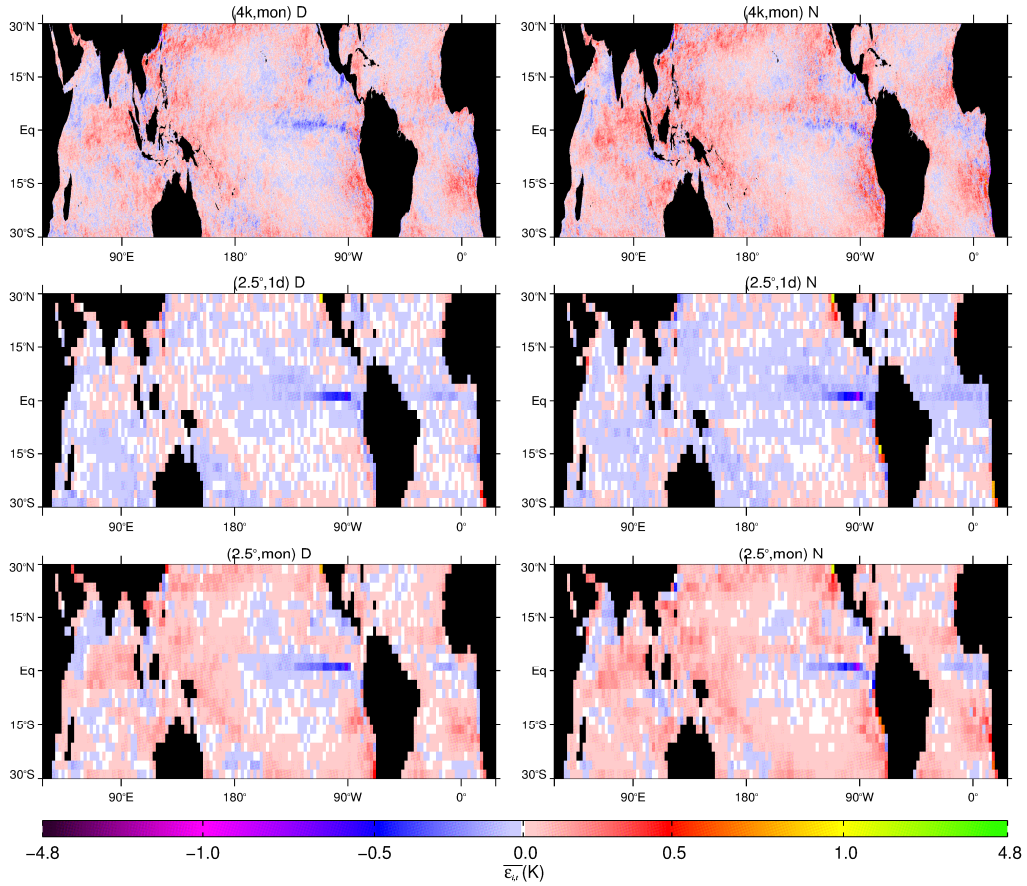

Figure 3.7 - Sampling errors introduced by clouds in infrared SSTs during the day (left) and at night (left). The top row shows the mean errors in monthly averaged daily fields at 4 km spatial resolution; the middle row shows the effects of spatial averages to 2.5° grid cells, and the bottom row shows spatially and temporally averaged fields. Note the color scale is non-linear (from Lui and Minnett, 2013).

GTMBA near-surface temperature measurements have been shown to provide valuable information for the assessment of uncertainties and stability of satellite-derived SSTs. The equatorial regions are absent in the measurements from drifting buoys and even the next generation of drifters that are expected to provide more accurate measurements will not render the GTMBA data unnecessary for satellite SST validation. The ITCZ results in poorer sampling in both infrared and microwave SSTs than in many other ocean regions, and the effects of clouds introduce significant errors in spatially and temporally averaged fields. Despite their respective limitations, satellite and in-situ SST measurements are complementary to each other to provide indispensible resources for the climate research community.

3.2 Altimeter and scatterometer calibration and validation

There is a clear need to maintain and even enhance the observing system over the global oceans and in particular over the Tropical Oceans. At the moment, weather centers all over the world are experiencing a dramatic decrease in the amount of in-situ tropical Pacific observations received through the Global Telecommunication System (GTS). Although it is often assumed currently that ample quantities of satellite observations are available for initialization and validation of weather and marine (i.e. both ocean-wave and ocean circulation) forecasts, in-situ

observations still play a crucial role. Firstly, subsurface observations can only be obtained from in-situ observations. Secondly, in-situ observations of air temperature, humidity, surface pressure and surface vector wind in the Tropical Pacific play an important role in weather analysis and in short-term weather forecasts. This is discussed extensively in the TPOS 2020 whitepaper on Operational Forecasting Systems. Thirdly, as discussed below, in-situ observations play a vital role in the development of a reliable geophysical model function (GMF) for satellite estimates of surface winds. Two examples are discussed next to illustrate this point, namely the development of GMFs for altimeter wind speeds and for scatterometer vector winds based on the efforts by the Royal Netherlands Meteorological Institute (KNMI). Finally, using a triple collocation technique which involves the collocation of three independent estimates of the truth, e.g. model forecast winds, scatterometer or altimeter winds and in-situ wind observations, allows estimation of the random error of each of the three collocated wind products. The availability of independent in-situ observations therefore gives important information on the quality of model and satellite products.

3.3 Development of a GMF for Altimeter and Scatterometer winds

Altimeters and scatterometers transmit microwave radiation to the wind-roughened ocean surface and measure the backscattered power. Altimeters are nadir-looking instruments, for which specular reflection of transmitted power leads to an inverse relation between backscatter and wind speed. Scatterometers, on the other hand, operate at oblique incidence angles in which the dominant scattering mechanism is the resonant interaction of the incident microwaves with short ocean ripple waves satisfying the Bragg resonance condition. These short waves are usually in equilibrium with the surface wind. Even though the physics of these backscatter processes are fairly well understood, wind retrievals from radar backscatter for both altimeter and scatterometer rely on empirical algorithms. A number of established approaches empirically relate radar backscatter to wind speed in the case of altimeters (e.g., Abdalla, 2012) and to the wind vector in the case of scatterometers (e.g., Hersbach, 2010; Ricciardulli and Wentz, manuscript in preparation).

3.4 Triple Collocation Analysis Using Satellite and In-situ Data

In the development of the GMF's the implicit assumption has been made that the in-situ observations or the model represent the truth. This is not necessarily the case, even for in-situ observations and therefore this assumption needs to be checked.

The observation error consists of several components. The instrumental error usually only gives a small contribution to the total error. More significant are the representation error and errors caused by the finite distance and time between to observations. The plausible reasons for model error have already been indicated.

When comparing several types of data it is desirable to have an idea about the size of the error. For example, when calibrating one instrument against another it is important to know their errors because the calibration constants depend on them. An example of linear regression is discussed by Marsden (1999). Furthermore, data assimilation requires knowledge of the weights given to the observations and to the first-guess field. These weights typically depend on the ratio of the first-guess error and the observation error. Therefore the resulting analysis will

depend on this ratio as well.

The need for estimating errors from different data sources was noted by Stoffelen (1998). He proposed to use a triple collocation method to calibrate observations of winds from the Scatterometer using winds from buoys, model winds and winds from the ERS-1 Scatterometer. If the errors of these data sources are uncorrelated it can be shown that the random error for each of them can be obtained. Assuming that one data source (e.g. the buoy winds) gives an unbiased estimate of the truth, the systematic errors of the other two can be obtained as well.

In a similar vein, Caires and Sterl (2003) applied a triple collocation method to estimate and calibrate winds and wave heights from the ERA40 analysis effort. In a somewhat different context, Tokmakian and Challenor (1999) estimated errors in the mean sea-level anomalies of model and the ERS-2 and Topex-Poseidon satellites. The triple collocation method has recently also be applied to validate the retrieval of soil moisture from Scatterometer data over land (Scipal et al., 2008). For a further discussion of the method, including some applications, see Janssen et al. (2007).

Abdalla et al. (2011) have extended this approach to estimate the errors in Altimeter wind and wave products as function of wind speed and wave height respectively. The overall statistics are as follows: the Envisat, Jason-1, buoys and 1-day forecast random error are 0.9, 1.0, 1.2, and 1.0 m/s while the scatter index (defined as the random error normalized with the mean value) for significant wave height for Envisat, Jason-1, buoys and first-guess wave height are 6%, 8%, 9% and 8%. These results suggest, on the one hand, that present day wind-wave forecasting is of high quality, while, on the other hand it should be clear that in-situ observations still play a vital role in assessing the quality of satellite and wind-wave model products. Finally, the high quality of the Satellite wind products should be stressed, in particular the Altimeter wind speed product and the Scatterometer wind vector. Combining the results from the comparison of the Advanced Scatterometer (ASCAT) wind speed with ECMWF winds, which typically gives a standard deviation of error of about 1.3 m/s (Hersbach, 2010), with the present estimate of the ECMWF wind speed error of 1 m/s, and suggests a quite low standard deviation error of about 0.6 m /s. This is in agreement with earlier results of Stoffelen (1998). In summary, the triple collocation method demonstrates the complementary use of satellite and in-situ data in error analysis. A triple collocation analysis involving satellite and in-situ data is also used in the validation and error analysis of Aquarius-derived SSS (ftp://podaac-ftp.jpl.nasa.gov/allData/aquarius/docs/v2/AQ-014-PS-0016AquariusSalinity -DataValidationAnalysis_DatasetVersion2.0.pdf).

3.5 QuikSCAT calibration and validation

QuikSCAT has provided an uninterrupted 10+ year record of vector winds over most of the rain and ice-free global ocean spanning the period July 19, 1999 to Nov 21, 2009. Compared to TAO winds, the rain-free QuikSCAT winds exhibited unprecedented accuracy. Distributions of the rain-free 10-m equivalent neutral wind (ENW) from QuikSCAT and all TAO buoys (solid and dashed lines in Figure 3.8 a-b, respectively) collocated in space and time over the complete QuikSCAT data record agree well. The percentage of QuikSCAT wind direction observations with absolute differences >90° are limited to light winds where there are relatively few observations (Figure 3.8 c). Between 3 and 9 m s^{-1}, the mean QuikSCAT wind speeds match very closely with the buoy wind speeds, as shown from the binned scatterplot in Figure 13d. For

wind speeds greater than 9 m s^{-1}, the QuikSCAT wind speeds are biased low compared to those from TAO (winds with speed higher than 9 m s^{-1} is often associated with rain in this region). The root-mean-square (RMS) differences between collocated QuikSCAT and TAO wind directions and wind speeds are shown in Figure 3.8 e-f, respectively, as a function of buoy wind speed. The RMS difference of wind direction shows a strong dependence on wind speed, with differences largest for small wind speeds, while decreasing rapidly as the wind speed increases. For the whole range of wind speeds, the overall RMS difference of wind direction is 26°, while restricted to wind speeds greater than 3 m s^{-1}, the RMS difference is 16°. The RMS wind speed differences also exhibit a significant dependence on wind speed, with the smallest RMS differences occurring between 6 and 9 m s^{-1}. Over the full range of wind speeds, the RMS difference in the 10-m ENW speed is 0.90 m s^{-1} for all buoys locations. Where both the buoys and QuikSCAT measure winds, they agree very well.

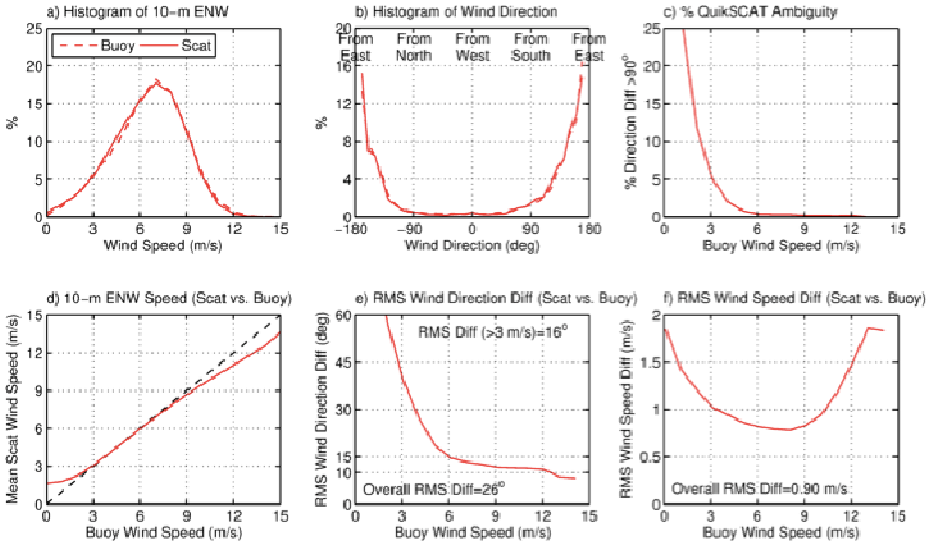

Figure 3.8 - Statistics for the comparison between collocated QuikSCAT and TAO 10-m ENW for all buoy locations over the 10+ year period July 19, 1999-Nov 21, 2009: (a) Histograms of wind speed (a) and direction (b) from QuikSCAT (solid) and TAO (dashed); (c) Percentage of QuikSCAT wind observations within each wind speed bin whose absolute wind direction differed from TAO by >90°; (d) QuikSCAT wind speed (y-axis) bin-averaged as a function of TAO wind speed (x-axis); RMS difference between QuikSCAT and TAO wind direction (e) and wind speed (f) on the y-axis as functions of buoy wind speed (x-axis). Only rain-free QuikSCAT wind observations were used in computing these statistics.

Rain can limit full utilization of QuikSCAT surface winds since rain degrades the ability of Ku-band scatterometers such as QuikSCAT and OSCAT to retrieve accurate vector winds over the ocean. Rain is relatively frequent in the western equatorial Pacific and along the ITCZ and western SPCZ, contaminating more than 30% of wind observations, as demonstrated in Figure 14a, which shows the percentage of rain-flagged QuikSCAT wind observations over the 10-yr period Aug 1999-Jul 2009. The northern and western TAO moorings (squares in Fig. 3.9 a) are well placed to measure winds in these rainy locales that are not measured accurately by satellite. Rarely does rain occur over the equatorial cold tongue and the southeast equatorial Pacific (<5% of the time). Such locations will be important for training wind retrieval algorithms

to account for rain and to determine when rain corrections can be done effectively. Figure 3.9 b-e show that rain frequency has strong seasonal variability over most of the TAO moorings.

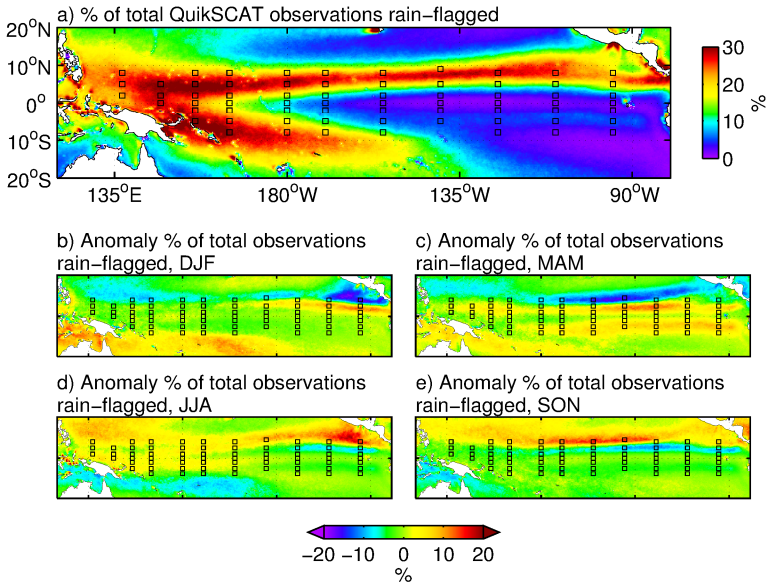

Figure 3.9 - (a) Map of the QuikSCAT rain-flag frequency over the 10-yr period August 1999-July 2009 from the Remote Sensing Systems (RSS) QuikSCAT version 4 dataset. (b-e) Seasonal anomalies of the QuikSCAT rain-flag frequency relative to total field in panel (a). Rain is determined from the QuikSCAT-only rain flag and collocated radiometer rain rate provided in the RSS dataset. The squares in each panel show the locations of the individual buoys in the TAO/TRITON array.

In light of the strong spatial and temporal rain variability, in situ TAO wind measurements are valuable in the tropical Pacific since anemometers provide all-weather sampling of surface winds. To demonstrate possible sampling limitations of scatterometer winds due to rain, the all-weather sampling capabilities of the TAO winds are exploited by computing the ratio of variances of rain-free and all-weather time series of zonal U10n and meridional V10n wind components at each buoy location shown in Figure 3.9. Figure 3.10 a,b shows this variance ratio as a function of time-scale. For time-scales less than 5 days, the rain-free time series contain significantly less variance than the all-weather time-series, while for longer than 5 days, the rain-free and all-weather variances are nearly equal. TAO wind measurements thus provide important information on temporal variability on time-scales less than 5 days that is degraded significantly in rain-free sampling, such as provided by most QuikSCAT wind datasets.

As shown in Figure 3.10 c-d, the variance reduction from rain-free sampling is strongly related to rain frequency for periods less than 3 days (black points); frequent rain strongly reduces measured wind variance. For rain frequencies greater than 20%, rain-free sampling captures only about half of the variance of the full all-weather time series. Even relatively modest occurrences of rain, 5% for example, reduces the measured wind variance to only about 80% of the all-weather wind variance. Rain still affects wind variability on time-scales of 3-5 days (red points), although less so; for periods greater than 5 days (green points), the variance ratios approach unity for the whole range of rain frequencies encountered. The effect on time-scales less than 5 days is a consequence of the intermittent nature of precipitating weather disturbance in the tropics.

In addition to the variance reduction at time-scales less than 5 days, cross-correlations between the rain-free QuikSCAT and TAO wind components are reduced below 0.8 on time-scales less than 5 days (Figure 3.10 e-f). Winds for both platforms are highly correlated for longer time-scales, however. Part of the drop-off in correlation for shorter time-scales is due to random instrument errors for each platform, but part is also due to errors in the satellite rain-flag, which is known to misidentify rain-contaminated grid cells (e.g., Weissman et al., 2012).

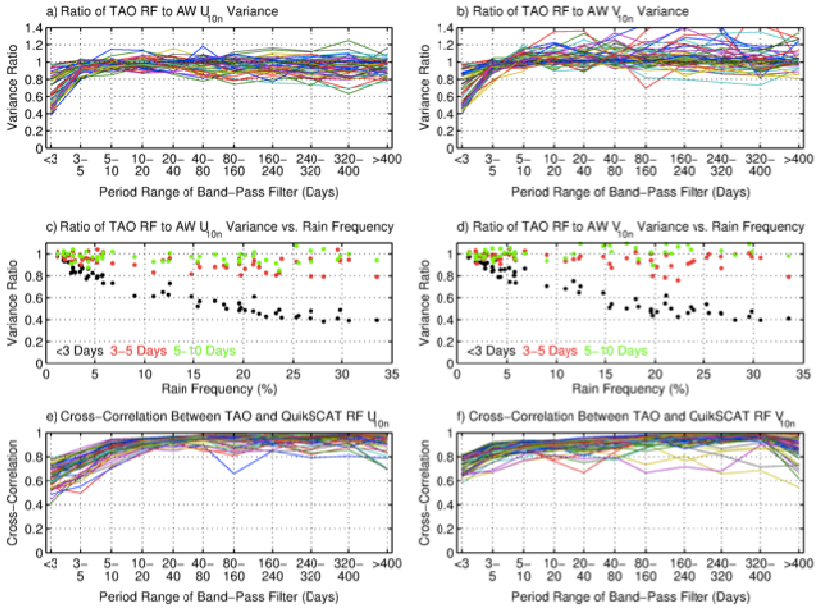

Figure 3.10 - Wind statistics computed over the 10-yr period August 1999-July 2009: (panels a-b) The ratio of temporal variance between rain-free (RF) and all-weather (AW) TAO equivalent neutral wind (ENW) components as a function of band-pass filtered time period. Each line corresponds to each of the buoys shown in Figure 2.2. (panels c-d) Ratio of TAO rain-free to all-weather wind variances as a function of rain-frequency for each buoy. Black points denote periods less than 3 days, red points are periods of 3-5 days, and green points are periods of 5-10 days. Each point represents an individual buoy. (panels e-f) Cross-correlation coefficients between the rain-free TAO and QuikSCAT ENW components as a function of band-pass filtered period. Each line corresponds to a different buoy. In all panels, only TAO winds collocated in time and space with QuikSCAT observations were used, and rain occurrence was determined from the QuikSCAT rain flag.

Despite that this analysis is based on the worst-case assumption of no useful data during rain, qualitatively similar problems exist within the JPL v3 QuikSCAT wind dataset for which corrections for rain were attempted. While this analysis demonstrates some limitations of rain-free sampling by QuikSCAT, it also shows that QuikSCAT provides accurate surface wind measurements for time-scales greater than approximately 5 days compared to those from TAO. Analysis of many of the wind-forced phenomena in the equatorial Pacific discussed earlier, such as ENSO, MJO, and TIWs, thus are not affected greatly by the rain-free QuikSCAT wind sampling.

In addition to the Cal/Val of the QuikSCAT wind fields, the satellite wind-SST interaction discussed in Section 2 has also been compared with that from the TAO mooring array (O'Neill 2012). The metric used for the comparison relies on the slope of the linear response of the

surface wind speed to SST perturbations along the equator. Figure 16 shows a bar chart comparing the ENW coupling coefficients estimated from both QuikSCAT and TAO (brown and green bars, respectively); these were estimated by binning the ENW and SST differences between pairs of buoys located along 2°S, 2°N, and the equator at 5 different longitudes. The coupling coefficients between QuikSCAT and the TAO buoys agree to within 10-30% at these locations, providing an independent verification of the QuikSCAT ENW response to SST.

The response of the QuikSCAT ENW may be due to either SST-induced changes to the actual wind speed, or to changes in surface layer stability that can change the surface stress without a change in wind speed. To determine the importance of each effect, the coupling coefficients for the response of the in situ buoy wind speed to SST are shown by the grey bars in Figure 3.11. These are about 20% smaller than the ENW coupling coefficients, which indicates that the wind response to SST observed by satellite is caused mainly by the response of the actual surface wind speed to SST rather than a simple adjustment of the surface layer stability. The in situ wind measurements from the TAO buoys thus provided an important clarification to the mechanisms involved in the satellite wind response to SST.

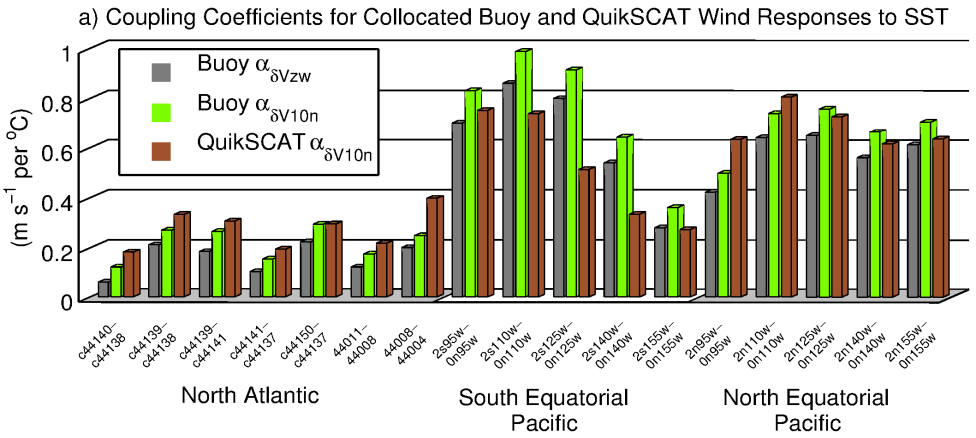

Figure 3.11 - Bar chart showing the coupling coefficients for the linear response of the 10-m ENW from QuikSCAT (brown) and the TAO buoys (green) to SST from the buoy pairs collocated spatially and temporally with the QuikSCAT ENW and AMSR-E SST. The grey bars show the linear coupling coefficients for the response of the in situ TAO winds to SST following the same procedure.

Recommendation: Ensure satellites are considered an integrated component of the tropical Pacific observing system. This should minimally include calibration/validation synergies with in situ systems, science and operational application contributions, and their role in tracking global climate teleconnections.

4. Enhancement of future satellite observing systems to complement the design of the future TPOS

Satellites are an important element of the integrated tropical Pacific observing system. Despite the significant achievement of satellite observations in the past few decades in understanding the variability of the tropical Pacific Ocean and related climate variability, there are several areas where improvement are required in order to advance these understanding further and to

improve the prediction of tropical Pacific climate variability. These include (1) the improvement of spatial and temporal sampling, (2) maintaining the continuity of satellite observations of Essential Ocean Variables (EOVs) and Essential Climate Variables (ECVs), and (3) expanding the variables measured from space (such as ocean surface current and mixed-layer depth). As an example of enhance of spatial sampling, the planned Surface Water Ocean Topography (SWOT) mission is designed to provide high-resolution SSH measurements that will revolutionize our ability to study meso- and sub-mesoscale variability of the ocean (in addition to its capability to capture terrestrial water bodies). The RapidSCAT, scheduled for launch to the International Space Station in June 2014, along with other scatterometers currently in orbit (e.g., ASCAT, OSCAT) and for the future will allow the study of diurnal wind in the tropics. JASON-3 and GRACE Follow-on continue the measurements of sea level and gravity beyond TOPEX/Poseidon, JASON-1 and -2, and GRACE. These future measurements will significantly bolster the capability of the integrated tropical Pacific observing system.

Recommendation: TPOS design should plan for the improved observations at air-sea interface resulting from approved satellite missions of the coming decade.

5. Conclusion

As an integral component of the tropical Pacific observing system, satellites have provided measurements for a suite of variables (SST, SSS, SSH, wind and wind stress, precipitation, significant wave height, and related derived products such as ocean surface current). These measurements and products have the great advantage and benefit of providing global context and uniform spatio-temporal sampling. They have significantly advanced our understanding of the tropical Pacific Ocean and related climate variability. Satellite observations are complementary to in-situ observations in many ways. They help decipher signals that are not adequately resolved or covered in space and time by in-situ observations. Together they provide a much more complete view of the three-dimensional structure of the ocean circulation and greatly benefit the study of air-sea interaction. Blended satellite and in-situ observations (e.g., SST and in the future, blended SSS) provide important value-added products that are important to the climate research community. In-situ and satellite observing systems work in tandem to illuminate phenomena of interest to both science and applications. Recent decades of research and applications demonstrate the value and synergy of a tropical Pacific observing system that takes advantage of latest satellite and in situ measurement technologies. Any new “design” of a tropical Pacific observing system must incorporate satellite remote sensing capabilities into the system.

References

Abdalla, S., Janssen, P.A.E.M., and Bidlot, J.R. (2011): Altimeter near real time wind and wave products: Random error estimation. Mar. Geod., 34, pp. 393-406.

Abdalla, S. (2012): Ku-Band Radar Altimeter Surface Wind Speed Algorithm. Mar. Geod., 35 (S1), pp. 276-298.

Boening, C., Willis, J.K., Landerer, F.W., Nerem, R.S., and Fasullo, J. (2012): The 2011 La Niña - So Strong, the Oceans Fell. Geophys. Res. Lett., 39, L19602, (doi:10.1029/2012GL053055).

BIPM (1995) : Comptes rendus de la 20^{e} Conférence Générale des Poids et Mesures, (CGPM). (Available at http://www.bipm.org/en/CGPM/db/20/1).

Caires, S., and Sterl, A. (2003): Validation of ocean wind and wave data using triple collocation. J. Geophys. Res., 108 (C3), pp. 3098, (doi:10.1029/2002JC001491).

Castro, S. L., Wick, G.A., and Buck, J.J.H. (2014): Comparison of diurnal warming estimates from unpumped Argo data and SEVIRI satellite observations. Remote Sens. Environ. 140(0): pp. 789-799.

Chelton, D. B., Wentz, F.J., Gentemann, C.L., de Szoeke, R.A., and Schlax, M.G. (2000): Satellite microwave SST observations of transequatorial tropical instability waves. Geophys. Res. Lett., 27, pp. 1239-1242.

Chelton, D. B., Esbensen, S.K., and Schlax, M.G. (2001): Observations of coupling between surface wind stress and sea surface temperature in the eastern Tropical Pacific. J. Climate, 14, pp. 1479-1498.

Chelton, D. B., Schlax, M.G., Lyman, J.M., and Johnson, G.C. (2003): Equatorially trapped Rossby waves in the presence of meridionally sheared baroclinic flow in the Pacific Ocean. Progress in Oceanography, 56, pp. 323-380.

Chelton, D. B. (2005): The impact of SST specification on ECMWF surface wind stress fields in the eastern tropical Pacific. J. Climate, 18, pp. 530-550.

Cravatte, S., Picaut, J., and Eldin, G. (2003): Second and first baroclinic Kelvin modes in the equatorial Pacific at intraseasonal timescales. J. Geophys. Res. 108, (doi: 10.1029/2002JC001511).

Donlon, C., Robinson, I.S., Reynolds, M., Wimmer, W., Fisher, G., Edwards, R., and Nightingale, T.J. (2008): An Infrared Sea Surface Temperature Autonomous Radiometer (ISAR) for Deployment aboard Volunteer Observing Ships (VOS). J. Atmos. Oceanic Tech., 25(1): pp. 93-113.

Donohue, K., and Wimbush, M. (1998): Model results of flow instabilities in the tropical Pacific Ocean. J. Geophys. Res., 103, (doi: 10.1029/98JC01912).

Durland, T. S., Samelson, R.M., Chelton, D.B., and de Szoeke, R.A. (2011): Modification of long Rossby wave phase speeds by zonal currents. J. Phys. Oceanogr., 41, pp. 1077-1101.

Durland, T. S., and Farrar, J.T. (2012): The wavenumber-frequency content of resonantly excited equatorial waves. J. Phys. Oceanogr., 42, pp. 1834-1858.

Embury, O., and Merchant, C.J. (2012a): A reprocessing for climate of sea surface temperature from the along-track scanning radiometers: A new retrieval scheme. Remote Sens. Environ. 116(0), pp. 47-61.

Embury, O., Merchant, C.J., and Filipiak, M.J. (2012b): A reprocessing for climate of sea surface temperature from the along-track scanning radiometers: Basis in radiative transfer. Remote Sens. Environ. 116(0): pp. 32-46.

Enfield, D. B. (1987): The intraseasonal oscillation in eastern Pacific sea levels: How is it forced? J. Phys. Oceanogr., 17, pp. 1860-1876.

Farrar, J. T. (2008): Observations of the dispersion characteristics and meridional sea-level structure of equatorial waves in the Pacific Ocean. J. Phys. Oceanogr., 38, pp. 1669-1689.

Farrar, J. T. (2011): Barotropic Rossby waves radiating from tropical instability waves in the Pacific Ocean. J. Phys. Oceanogr., 41, pp. 1160-1181.

Gentemann, C. L., Wentz, F.J., Mears, C.A., and Smith, D.K. (2004): In situ validation of Tropical Rainfall Measuring Mission microwave sea surface temperatures. J. Geophys. Res., 109(C4): C04021.

Halpern, D., Knox, R.A., and Luther, D. (1988): Observations of the 20-day period meridional current oscillations in the upper ocean along the Pacific equator. J. Phys. Oceanogr., 18, pp. 1514-1543.

Hashizume, H., Xie, S.P., Liu, W.T., and Takeuchi, K. (2001): Local and remote atmospheric response to tropical instability waves: A global view from space. J. Geophys. Res., 106, pp. 10173–10185.

Hersbach, H. (2010): Comparison of C-Band Scatterometer CMOD5.N Equivalent Neutral Winds with ECMWF. J. Atmos. Oceanic Technol., 27, pp. 721-736.

Interim Sea Surface Temperature Science Team (2010): Sea Surface Temperature Error Budget: White Paper. Available at http://www.sstscienceteam.org/white_paper.html.

Johnson, G. C. (1993): A deep inertial jet on a sloping bottom near the equator. Deep-Sea Res. I, 40, 1781-1792, (doi:10.1016/0967-0637(93)90032-X).

Hendon, H. H., Liebmann, B., and Glick, J.D. (1998): Oceanic Kelvin waves and the Madden-Julian Oscillations. J. Atmos. Sci., 55, pp. 88-101.

Janssen, P.A.E.M., Abdalla, S., Hersbach, H., and Bidlot, J. (2007): Error estimation of buoy, satellite and model wave height data. J. Atmos. Oceanic Technol., 24, pp. 1665-1677.

Johnson, G. C., and McPhaden, M.J. (1993): Effects of a 3-dimensional mean flow on intraseasonal Kelvin Waves in the Equatorial Pacific Ocean. J. Geophys. Res., 98, pp. 10185-10194.

Kaiser-Weiss, A., Vazquez, J., and Chin, M. (2012): GHRSST User Requirements Document (URD), Version 2.0. National Centre for Earth Observation, Dept. Meteorology, University of Reading, Reference D-06 URD_v02, 42 pp.

Kessler, W. S. and McCreary, J.P. (1993): The annual wind-driven Rossby wave in the sub-thermocline equatorial Pacific. J. Phys. Oceanogr., 23, pp. 1192-1207.

Kessler, W. S. and M. J. McPhaden, 1995: Oceanic equatorial waves and the 1991-93 El Niño. J. Climate, 8, 1757-1774.

Kessler, W. S., McPhaden, M.J., and Weickmann, K.M. (1995): Forcing of intraseasonal Kelvin waves in the equatorial Pacific. J. Geophys. Res., 100, pp. 10613-10631.

Kessler, W. S., Johnson, G.C., and Moore, D.W. (2003): Sverdrup and Nonlinear Dynamics of the Pacific Equatorial Currents. J. Phys. Oceanogr., 33, pp. 994–1008.

Kutsuwada, K., and McPhaden, M.J. (2002): Intraseasonal Variations in the Upper Equatorial Pacific Ocean prior to and during the 1997–98 El Niño. J. Phys. Oceanogr., 32, pp. 1133–1149.

Lagerloef, G.S.E, Lukas, R., and Bonjean, F. (2003): El Niño tropical Pacific Ocean surface current and temperature evolution in 2002 and outlook for early 2003. Geophys. Res. Lett., 30, (doi:10.1029/2003GL017096).

Lee, T., and M. J. McPhaden, 2008: Decadal phase change in large-scale sea level and winds in the Indo-Pacific region at the end of the 20th century. Geophys. Res. Lett., 35, L01605, doi:10.1029/2007GL032419.

Lee, T., and McPhaden, M.J. (2010): Increasing intensity of El Niño in the central-equatorial Pacific. Geophys. Res. Lett., 37, L14603, (doi:10.1029/2010GL044007).

Lee, T., Hobbs, W., and Willis, J. (2010): Record warming in the South Pacific and western Antarctica associated with the strong central-Pacific El Niño in 2009-10. Geophys. Res. Lett., 37, L19704, (doi:10.1029/2010GL044865).

Lee, T., Lagerloef, G., Gierach, M.M., Kao, H.Y., Yueh, S.S. and Dohan, K. (2012): Aquarius reveals salinity structure of tropical instability waves. Geophys. Res. Lett., 39, L12610, (doi:10.1029/2012GL052232).

Legeckis, R.V. (1977): Long waves in the eastern equatorial ocean. Science, 197, pp. 1177–1181.

Liu, W. T., Xie, T.X., Polito, P.S., Xie, S.P., and Hashizume, H. (2000): Atmospheric Manifestation of Tropical Instability Wave Observed by QuikSCAT and Tropical Rain Measuring Mission. Geophys. Res. Lett., 27, pp. 2545-2548.

Lui, Y., and Minnett, P.J. (2013): Sampling Errors in Satellite Derived Sea Surface Temperature for Climate Data Records. Presented at 14th Science Team Meeting of the Group for High Resolution Sea-Surface Temperature. Woods Hole. 17 – 21 June 2013.

Lukas, R., and Firing, E. (1985): The annual Rossby wave in the Central Equatorial Pacific Ocean. J. Phys. Oceanogr., 11, pp. 55-67.

Lumpkin, R., Goni, G., and Dohan, K. (2013): Surface Currents, in "State of the Climate in 2012". Bull. Amer. Meteor. Soc., 94, S62-S65. (doi: 10.1175/2013BAMSStateoftheClimate.1).

Luther, D. S., and Johnson, E.S. (1990): Eddy energetics in the Upper Equatorial Pacific during the Hawaii-to-Tahiti Shuttle Experiment. J. Phys. Oceanogr., 20, pp. 913-944.

Lyman, J. M., Chelton, D.B., de Szoeke, R.A., and Samelson, R.M. (2005): Tropical Instability Waves as a Resonance between Equatorial Rossby Waves. J. Phys. Oceanogr., 35, pp. 232–254.

Lyman, J. M., Johnson, G.C., and Kessler, W.S. (2007): Distinct 17- and 33-Day Tropical Instability Waves in Subsurface Observations. J. Phys. Oceanogr., 37, pp. 855–872.

Madden, R. A., and Julian, P.R. (1994): Observations of the 40–50-day tropical oscillation—A review. Mon. Wea. Rev, 122, pp. 814–837.

McPhaden, M. J. (1996): Monthly period oscillations in the Pacific North Equatorial Countercurrent. J. Geophys. Res., 101, 6337-6359, (doi:10.1029/95JC03620).

McPhaden, M. J., and Taft, B.A. (1988): Dynamics of Seasonal and Intraseasonal Variability in the Eastern Equatorial Pacific. J. Phys. Oceanogr., 18, pp. 1713–1732.

McPhaden, M. J., Busalacchi, A.J., Cheney, R., Donguy, J.R., Gage, K.S., Halpern, D., Ji, M., Julian, P., Meyers, G., Mitchum, G.T., Niiler, P.P., Picaut, J., Reynolds, R.W., Smith, N., and Takeuchi, K. (1998): The Tropical Ocean-Global Atmosphere observing system: A decade of progress. J. Geophys. Res., 103, pp. 14169-14240.

Merchant, C. J., Embury, O., Rayner, N.A., Berry, D.I., Corlett, G.K., Lean, K., Veal, K.L., Kent, E.C., Llewellyn-Jones, D.T., Remedios, J.J., and Saunders, R. (2012): A twenty-year independent record of sea surface temperature for climate from Along Track Scanning Radiometers. J. Geophys. Res. 117.

Minnett, P. J. (2010): The Validation of Sea Surface Temperature Retrievals from Spaceborne Infrared Radiometers. Oceanography from Space, revisited. V. Barale, J. F. R. Gower and L. Alberotanza, Springer Science+Business Media B.V.: pp. 273-295.

Minnett, P. J., and Corlett, G.K. (2012): A pathway to generating Climate Data Records of sea-surface temperature from satellite measurements. Deep Sea Res. Part II, 77–80(0): pp. 44-51.

Minnett, P. J., Knuteson, R.O., Best, F.A., Osborne, B.J., Hanafin, J.A., and Brown, O.B. (2001): The Marine-Atmospheric Emitted Radiance Interferometer (M-AERI), a high-accuracy, sea-going infrared spectroradiometer. J. Atmos. Oceanic Tech., 18(6): pp. 994-1013.

Moore, D. W., and Philander, S.G.H. (1977): Modeling of the Tropical Ocean Circulation. In “The Sea,” Vol. 6, pp. 319–361 (Goldberg et al., ed.). Wiley, New York.

NRC (2000): Issues in the Integration of Research and Operational Satellite Systems for Climate Research: II. Implementation. Washington, DC, National Academy of Sciences.

NRC (2004): Climate Data Records from Environmental Satellites. Washington, DC. National Academy of Sciences.

O'Carroll, A. G., Eyre, J.R., and Saunders, R.W. (2008): Three-Way Error Analysis between AATSR, AMSR-E, and In Situ Sea Surface Temperature Observations. J. Atmos. Oceanic Tech., 25(7): pp. 1197-1207.

O'Carroll, A. G., Blackmore, T., Fennig, K., Saunders, R.W., and Millington, S. (2012): Towards a bias correction of the AVHRR Pathfinder SST data from 1985 to 1998 using ATSR. Remote Sens. Environ. 116(0): pp. 118-125.

Ohring, G., Wielicki, B., Spencer, R., Emery, B., and Datla, R. (2005): Satellite Instrument Calibration for Measuring Global Climate Change: Report of a Workshop. Bull. Amer. Meteor. Soc., 86(9): pp. 1303-1313.

Pezzi, L. P., Vialard, J., Richards, K., Menkes, C., and Anderson, D. (2004): Influence of ocean-atmosphere coupling on the properties of tropical instability waves. Geophys. Res. Lett., 31, (doi: 10.1029/2004GL019995).

Picaut, J., Loualalen, M., Menkes, C., Delcroix, T., and McPhaden, M.J. (1996): Mechanism of the Zonal Displacements of the Pacific Warm Pool: Implications for ENSO. Science, 274, pp. 1486-1489.

Perigaud, C. (1990): Sea level oscillations observed with Geosat along the two shear fronts of the Pacific North Equatorial Countercurrent. J. Geophys. Res., 95, pp. 7239-7248.

Philander, S. G. H. (1978): Instabilities of zonal equatorial currents, Part 2. J. Geophys. Res., 83, pp. 3679-3682.

Polito, P., Ryan, J., Liu, W.T., and Chavez, F.P. (2001): Oceanic and Atmospheric Anomalies of Tropical Instability Waves. Geophys. Res. Lett., 28, pp. 2233-2236.

O’Neill, L. W. (2012): Wind Speed and Stability Effects on Coupling between Surface Wind Stress and SST Observed from Buoys and Satellite. J. Climate, 25, pp. 1544-1569.

Qiao, L., and Weisberg, R.H. (1995): Tropical instability wave kinematics: Observations from the Tropical Instability Wave Experiment. J. Geophys. Res., 100, pp. 8677–8693.

Reynolds, R. W., Smith, T.M., Liu, C., Chelton, D.B., Casey, K., and Schlax, M.G. (2007): Daily high-resolution-blended analyses for sea surface temperature. J. Climate, 20, pp. 5473–5496.

Rice, J. P., J. J. Butler, B. C. Johnson, P. J. Minnett, Maillet, K.A., Nightingale, T.J., Hook, S.J., Abtahi, A., Donlon, C.J., and Barton, I.J. (2004): The Miami 2001 Infrared Radiometer Calibration and Intercomparison: 1. Laboratory Characterization of Blackbody Targets. J. Atmos. Oceanic Tech., 21, pp. 258-267.

Risien, C. M., and Chelton, D.B. (2008): A Global Climatology of Surface Wind and Wind Stress Fields from Eight Years of QuikSCAT Scatterometer Data. J. Phys. Oceanogr., 38, pp. 2379-2413.

Roundy, P. E., and Frank, W.M. (2004): A Climatology of Waves in the Equatorial Region. J. Atmos. Sci., 61, pp. 2105–2132.

Scipal, K., Holmes, T., de Jeu, R., Naeimi, V. and Wagner, W. (2008): A possible solution for the problem of estimating the error structure of global soil moisture data sets. Geophys. Res. Lett., 35, L24403, (doi:10.1029/2008GL035599).

Seo, H., Jochum, M., Murtugudde, R., Miller, A.J., and Roads, J.O. (2007): Feedback of Tropical Instability-Wave-Induced Atmospheric Variability onto the Ocean. J. Climate, 20, pp. 5842–5855.

Shinoda, T., Kiladis, G.N., and Roundy, P.E. (2009): Statistical representation of equatorial waves and tropical instability waves in the Pacific Ocean. Atmos. Res., 94, pp. 37–44.

Stoffelen, A. (1998): Error modeling and calibration: Towards the true surface wind speed. J. Geophys. Res. 103, pp. 7755-7766.

Tokmakian, R., and Challenor, P.G. (1999): On the joint estimation of model and satellite sea surface height anomaly errors. Ocean Modelling, 1, pp. 39-52.

Wakata, Y. (2007): Frequency-wavenumber spectra of equatorial waves detected from satellite altimeter data. J. Oceanogr., 63, pp. 483–490.

Wang, W. M., and McPhaden, M.J. (2001): Surface layer temperature balance in the Equatorial Pacific during the 1997–98 El Niño and 1998–99 La Niña. J. Climate, 14, pp. 3393–3407.

Weissman, D. E., Stiles, B.W., Hristova-Veleva, S.M., Long, D.G., Smith, D.K., Hilburn, K.A., and Jones, W.L. (2012): Challenges to Satellite Sensors of Ocean Winds: Addressing Precipitation Effects. J. Atmos. Oceanic. Tech., 29, pp. 356-384.

Wheeler, M., and Kiladis, G.N. (1999): Convectively Coupled Equatorial Waves: Analysis of Clouds and Temperature in the Wavenumber–Frequency Domain. J. Atmos. Sci., 56, pp. 374–399.

Willis, J. K., Roemmich, D., and Cornuelle, B. (2003): Combining altimetric height with broadscale profile data to estimate steric height, heat storage, subsurface temperature, and sea-surface temperature variability, J. Geophys. Res., 108 (C9), pp. 3292.

Willis, J. K., Chambers, D.P. and Nerem, R.S. (2008): Assessing the Globally Averaged Sea Level Budget on Seasonal to Interannual Time Scales. J. Geophys. Res., 113, C06015, (doi:10.1029/2007JC004517).

Willis, J. K. (2010): Can In-Situ Floats and Satellite Altimeters Detect Changes in Atlantic Ocean Overturning? Geophys. Res. Lett., 37, L06602, (doi:10.1029/2010GL042372).

Wimmer, W., Robinson, I.S., and Donlon, C.J. (2012): Long-term validation of AATSR SST data products using shipborne radiometry in the Bay of Biscay and English Channel. Remote Sens. Environ. 116(0): pp. 17-31.

Xu, F., and Ignatov, A. (2010): Evaluation of in situ sea surface temperatures for use in the calibration and validation of satellite retrievals. J. Geophys. Res., 115(C9): C09022.

Zang, X., Fu, L.L., and Wunsch, C. (2002): Observed reflectivity of the western boundary of the equatorial Pacific Ocean. J. Geophys. Res., 107, 3150, (doi:10.1029/2000JC000719).

Zhang, R.-H., and Busalacchi, A.J. (2008): Rectified effects of tropical instability wave (TIW)-induced atmospheric wind feedback in the tropical Pacific. Geophys. Res. Lett., 35, L05608. (doi:10.1029/2007GL033028).

Zhang, R.-H., and Busalacchi, A.J. (2009): An Empirical Model for Surface Wind Stress Response to SST Forcing Induced by Tropical Instability Waves (TIWs) in the Eastern Equatorial Pacific. Mon. Wea. Rev., 137, pp. 2021–2046.

Zhang, X. and McPhaden, M.J. (2010): Interannual surface layer heat balance in the eastern equatorial Pacific and its relationship with local atmospheric forcing. J. Climate, 23, pp. 4375–4394.